Progress In Electromagnetics Research B, Vol. 53, 333–354, 2013

TARGET DETECTION FROM MICROWAVE IMAGING BASED ON RANDOM SPARSE ARRAY AND COMPRESSED SENSING

Ling Huang* **and Yi Long Lu**

School of Electrical and Electronic Engineering, Nanyang Technological University, Singapore

Abstract—This paper proposes an imaging scheme using a random sparse array (RSA) structure for radar target detection using compressed sensing (CS). The array collects sparse measurements with less collection time and data storage. Two schemes of the RSA are considered, random SAR mode and random array mode. Performances of both static and moving target detections are investigated. Performance of RSA with CS is compared with that using full SAR data with conventional back-projection (BP) method for static target detection and full uniform linear array (ULA) data with conventional beamforming (CBF) method for moving target detection. Simulation and real experimental tests are provided to verify the proposed target imaging scheme. Results show that RSA imaging with CS can perform better than normal SAR and ULA with conventional imaging methods. However, when environment is complicated and background too noisy, CS may have degraded performance.

1. INTRODUCTION

Compressed sensing (CS) [1–3] is an emerging technology and attracting much attention in many research areas. It challenges Nyquist sampling theorem in signal processing. CS states that it is possible to perfectly recover sparse/compressible signals with highly incomplete information under proper transformation basis. This is very useful and attractive in areas requiring large amount of data processing time and storage, such as image to image processing, medical imaging and radar imaging including Synthetic Aperture Radar (SAR) imaging and Through Wall Radar Imaging (TWRI).

Received 17 May 2013, Accepted 10 August 2013, Scheduled 13 August 2013

* Corresponding author: Ling Huang (HUAN0231@e.ntu.edu.sg).

CS has been proved to be efficient especially in applications of radar imaging by many research works. In [4], Baraniuk and Steeghs introduced CS to radar imaging and successfully demonstrated its advantages in eliminating matched filtering and reducing receiver analog-to-digital conversion (ADC) bandwidth. In [5], Patel et al. introduced CS concept in SAR and presented an imaging modality with high-resolution map of the spatial distribution of targets and terrain using reduced number of transmitted/received signals. Wei et al. [6] presented a high resolution imaging method for SAR sparse targets reconstruction based on CS theory, which reduced sample size and avoided limitation in the resolution ability of conventional SAR imaging method based on matched filtering (MF) theory. In [7], CS was applied to both simulation data and experimental SAR raw data to demonstrate the effectiveness of CS on two separate 1-D processing operations in range and azimuth dimensions. Similarly in [8], Wei et al. applied CS to linear array SAR (LASAR) to obtain high resolution images and verified via both simulation and experimental data. Another novel imaging method proposed by Li et al. in [9] based on SAR and compressed sensing also outperforms conventional SAR imaging method with higher resolution, lower peak-sidelobe ratio and less sample data. Recently in [10], Yang et al. proposed a random-frequency SAR imaging scheme based on CS. Limitations of stepped-frequency SAR system can be overcome by transmitting only a small number of frequencies. At the same time, the available imaging range width is enlarged significantly with range and azimuth resolutions maintained. However, to the authors' knowledge, there are not many works on CS based random array processing.

The concept of random sparse array (RSA) was firstly presented in [11] for forming building images from different angles. Ao et al. [12] applied the RSA concept in multi-channel through-the-wall radar target imaging. Such a random sparse array is able to reduce the computational burden and operational complexity of an imaging system. Inspired by the ideas, we propose a RSA imaging scheme combined with CS for target detection with the aim of reducing operational complexity as well as data collection time and storage. The sparse property of RSA is able to satisfy the sparsity requirement of CS [13, 14]. We have investigated the performance of the proposed RSA scheme in both static and moving target detections. We present the image formation results based on CS and time-domain back-projection (BP) [15, 16] method and conventional beamforming (CBF) method for static and moving targets respectively. After that, static target detection based on CS is verified using real experimental data.

The rest of this paper is organized as follows. Section 2 gives the

review of CS and SAR imaging theory. In Section 3, CS algorithm based on RSA is described. Section 4 presents simulation results of target detections, including static and moving targets. Section 5 gives the respective experimental results. Finally, Section 6 concludes the entire paper.

2. COMPRESSED SENSING (CS) AND SAR IMAGE FORMATION

2.1. CS Theory

A vector $\mathbf{s}$ ($\mathbf{s} \in \mathbf{C}^N$) is called Q-sparse if the number of non-null elements in $\mathbf{s}$ is not larger than Q ($\|\mathbf{s}\|_0 \leq Q$, $\|\cdot\|_0$ represents the zero-norm (l_0 norm) which refers to the non-null elements in vector $\mathbf{s}$). It can be the vector representing a sparse scene with Q targets. Suppose another signal $\mathbf{x}$ is sparse on a basis matrix $\mathbf{\Psi}$ which represents a linear transformation. Signal $\mathbf{x}$ of length $N \times 1$ is also Q-sparse if it can be written in the form of (1).

$$\mathbf{x} = \mathbf{\Psi}\mathbf{s} \tag{1}$$

where $\mathbf{\Psi}$ is called the sparsifying matrix of size $N \times N$. Signal $\mathbf{x}$ is usually measured by a measurement vector $\mathbf{y}$ in a system. The measurement vector $\mathbf{y}$ of length $M \times 1$ ($M < N$) is a linear projection of $\mathbf{x}$ on a random matrix $\mathbf{\Phi}$,

$$\mathbf{y} = \mathbf{\Phi}\mathbf{x} \tag{2}$$

where $\mathbf{\Phi}$ is a $M \times N$ measurement matrix (where $M \ll N$). From (1) and (2) we can find the relationships between $\mathbf{y}$ and $\mathbf{s}$. Obviously $\mathbf{y}$ can be represented in terms of $\mathbf{s}$ via the following expression,

$$\mathbf{y} = \mathrm{A}\mathbf{s} \tag{3}$$

where $\mathbf{A} = \mathbf{\Phi}\mathbf{\Psi}$.

To recover $\mathbf{s}$ from $\mathbf{y}$, one needs to solve a minimization problem expressed in (4).

$$\min_{\mathbf{s}} \|\mathbf{s}\|_1 \text{ s.t. } \mathbf{y} = \mathbf{A}\mathbf{s} \tag{4}$$

where $\|\cdot\|_1$ represents the l_p norm having the classic definition of $\|\mathbf{s}\|_p = \left(\sum_{n=1}^{N} |s_n|^p\right)^{1/p}$ at $p = 1$. When noise is present, the problem becomes (5), and ξ is the uncertainty level.

$$\min_{\mathbf{s}} \|\mathbf{s}\|_1 \text{ s.t. } \|\mathbf{y} - \mathrm{A}\mathbf{s}\|_2 \leq \xi \tag{5}$$

It has been proved in [1–3] that in order to exactly recover the desired sparse vector $\mathbf{s}$ using $\mathbf{y}$, the transformation matrix $\mathbf{A}$ must satisfy the *Restricted Isometry Property (RIP).*

$$(1-\delta)\left\|\mathbf{s}\right\|_2 \leq \left\|\mathbf{A}\mathbf{s}\right\|_2 \leq (1+\delta)\left\|\mathbf{s}\right\|_2 \tag{6}$$

where δ is the smallest possible constant ($\delta > 0$). $\|\cdot\|_2$ represents the l_2 norm ($p = 2$). The RIP actually measures how well every set of Q columns of $\mathbf{A}$ forms approximately an orthonormal system. The smaller the positive constant δ is, the more possible to perfectly recover signals. The number of minimum measurements required is determined by the mutual coherence of matrix $\mathbf{\Phi}$ and $\mathbf{\Psi}$. Mutual coherence indicates the spreading extent of information associated with $\mathbf{s}$ among the entries of $\mathbf{y}$. The lower mutual coherence between $\mathbf{\Phi}$ and $\mathbf{\Psi}$ is, the fewer number of measurements are needed to recover $\mathbf{s}$ from $\mathbf{y}$ [17]. The required number of measurements to recover $\mathbf{s}$ must satisfy the condition stated in [18],

$$M \geq C\left[\mu\left(\mathbf{\Phi}, \mathbf{\Psi}\right)\right]^2 NQ\log Q \tag{7}$$

where C is a constant and $\mu(\mathbf{\Phi}\mathbf{\Psi})$ the mutual coherence between $\mathbf{\Phi}$ and $\mathbf{\Psi}$ of which the mathematical expression is,

$$\mu\left(\mathbf{\Phi}, \mathbf{\Psi}\right) = \max_{i\neq j}\left|\langle \mathbf{\Phi}_i, \mathbf{\Psi}_j\rangle\right| \tag{8}$$

where $\mathbf{\Phi}_i$ and $\mathbf{\Psi}_j$ are columns of the matrix and this expression is only valid if these columns have unit norms.

Several approaches are used in CS to reconstruct the sparse signal, such as convex optimization [19, 20] and greedy algorithms [21–24]. Among these approaches, Orthogonal Matching Pursuit (OMP) [22] is a widely used version of greedy algorithms and $\mathbf{s}$ can be recovered by iteratively finding global minimum from locally optimal solution in each step.

2.2. SAR Imaging

In conventional SAR imaging system, single sensor moves along the azimuth direction to transmit and receive signals at each azimuth sampling position. Uniform azimuth sampling position and large azimuth aperture are required to ensure FFT processing and good azimuth resolution respectively. Range resolution is ensured by using wideband signals such as linear frequency modulated (LFM) signal (such as chirp) or stepped-frequency signal. Stepped-frequency SAR synthesizes a wide bandwidth by transmitting large number of single frequency pulses. This requires large data storage and extensive processing time.

Suppose there are total M radar positions, Q targets in the scene and N number of frequency bins in the stepped-frequency signal. The starting frequency is f_0, frequency step is Δf. The transmitting signal with frequency f_n is expressed as,

$$s_n(t) = \text{rect}\left(\frac{t - T_p/2}{T_p}\right) \exp(j2\pi f_n t) \tag{9}$$

where $f_n = f_0 + (n-1)\Delta f$ and $\text{rect}(\frac{t-T_p/2}{T_p}) = u(t) - u(\frac{t-T_p}{T_p})$, $u(t)$ is the unit function.

Received echo signal is amplitude modulated and phase shifted version of the transmitting signal. The received echo signal from the qth target to the mth radar position is,

$$r_{mq}(n,t) = \sigma_q \text{rect}\left(\frac{t - \tau_{mq} - T_p/2}{T_p}\right) \exp[j2\pi f_n (t - \tau_{mq})] \tag{10}$$

where $\tau_{mq} = 2R_{mq}/c$. R_{mq} is the distance between the qth target and the mth radar position. σ_q denotes the reflectivity of the qth target. After frequency demodulation, lowpass filtering and digital sampling, the discrete baseband received signal at nth frequency and mth radar position is,

$$x[m,n] = \sum_{q=1}^{Q} \sigma_q \exp(-j2\pi f_n \tau_{mq}) + w[m,n] \tag{11}$$

where $w[m,n]$ represents the noise term. Therefore total baseband received signal at mth radar position is a vector of length $N \times 1$,

$$x[m] = [x[m,1] \;\; x[m,2] \;\; \ldots \;\; x[m,N]]^T \tag{12}$$

In matrix form, signal received at all the radar positions is expressed as an $N \times M$ matrix,

$$\mathrm{X} = [x[1] \;\; x[2] \;\; \ldots \;\; x[M]] \tag{13}$$

The imaging process of SAR includes range compression and azimuth compression. For stepped-frequency signal, range compression is realized by performing inverse discrete Fourier transform (IDFT) on received baseband signals, azimuth compression is normally achieved by back-projection (BP) algorithm.

3. COMPRESSED SENSING TARGET DETECTION USING RSA

3.1. Random Sparse Array (RSA)

In this section, we present the detailed geometry of the random sparse array as well as its implementations.

We characterize the RSA into two modes. One is called random SAR mode and the other called random array mode (see Fig. 1). SAR mode is similar to conventional SAR case — using single sensor for transmitting and receiving at each azimuth position. But the difference is that we randomly move the sensor to a position for transmitting and receiving. The distance between adjacent azimuth positions is random, and positions may be determined by inertial measurement units (IMU) with ring laser gyro or MEMS gyro [25, 26]. Array mode is similar to normal uniform linear array (ULA). Few number of antenna elements are randomly placed in a position. The elements are located randomly forming a large aperture array with very few elements. The element positions may be determined using above method. Along with the two modes, their respective comparable geometries are also illustrated in Fig. 1. To make the comparison reasonable, the first and the last elements of RSA are kept to be at the same position as that of the respective SAR/ULA geometry, elements in between are random located. From the schematic geometries, we can directly tell that RSA needs much fewer elements and measurements than normal SAR and ULA and is much easier to implement.

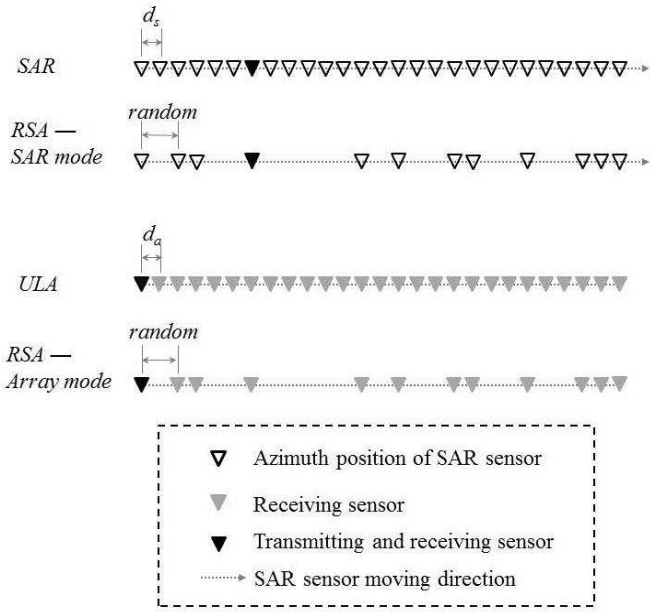

Figure 1. Schematic diagram of RSA schemes (SAR mode and array mode) and respective comparisons (SAR and ULA).

Assume that there are M random sparse positions or array elements in the system. The RSA can be denoted using a position matrix (14).

$$\mathbf{P} = [\mathbf{r}_0\ \mathbf{r}_1\ \ldots\ \mathbf{r}_m\ \ldots\ \mathbf{r}_{M-1}]^T \tag{14}$$

where $\mathbf{r}_0$ is the first azimuth position in RSA-SAR mode or the TX position in RSA-array mode. The first position vector $\mathbf{r}_0$ is fixed and the mth position vector can be expressed in (15).

$$\mathbf{r}_m = \mathbf{r}_{m-1} + \Delta x_m \mathbf{a}_x + \Delta y_m \mathbf{a}_y, \quad m = 1, 2, \ldots, M-1 \tag{15}$$

where $\mathbf{r}_m = x_m \mathbf{a}_x + y_m \mathbf{a}_y$, Δx_m and Δy_m are the distance displacements from the $(m-1)$th position along x axis and y axis, respectively. In this paper, we consider the case when the displacement occurs at one direction (along the sensor moving direction above) only.

3.2. Static Target Detection Using CS

In this section, we investigate the performance of the first scheme of RSA, random SAR mode, in which one sensor is used. We consider that a RSA has M random sparse positions, the sensor transmits a stepped-frequency signal and then receives it at each position, and the signal is composed of N frequency bins.

Assume that the investigated target scene is sparse. We divide the area into pixels of size $d_x \times d_y$, where $x = 1, 2, \ldots, K$, and $y = 1, 2, \ldots, L$. Reflectivity at (x, y)th pixel is σ_{xy}. Denote target scene reflectivity as a vector

$$\mathbf{s} = [\sigma_{11}, \sigma_{21}, \ldots, \sigma_{K1}, \sigma_{12}, \sigma_{22}, \ldots, \sigma_{xy}, \ldots, \sigma_{KL}]^T \tag{16}$$

where $\sigma_{xy} = 0$ if no target is in the (x, y)th pixel.

The received signal is related to the scene reflectivity by an amplitude modulation and phase shift as in (10). Let $g = x + (y-1)K$ [27], ranging from 1 to KL, the received signal at nth frequency and mth radar position without noise is expressed as,

$$x[m, n] = \sum_{g=1}^{KL} \sigma_g \exp(-j2\pi f_n \tau_{mg}) \tag{17}$$

where $\tau_{mg} = 2R_{mg}/c$. R_{mg} is the distance between mth radar position and gth pixel position.

The total measurement data are the summation of the received signal from each individual pixel position. Therefore, expressing the measurement data at all the azimuth positions in RSA in matrix format when R number of frequency bins are selected for processing, we get

$$\mathbf{y} = \mathbf{\Phi x} + \mathbf{w} = \mathbf{\Phi \Psi s} + \mathbf{w} \tag{18}$$

where

$$\begin{aligned}\boldsymbol{\Psi} &= \left[\boldsymbol{\Psi}_1^T\ \boldsymbol{\Psi}_2^T\ \ldots\ \boldsymbol{\Psi}_N^T\right]^T_{MN\times KL}\\ [\boldsymbol{\Psi}_n]_{mg} &= \exp(-j2\pi f_n \tau_{mg})\\ \tau_{mg} &= \frac{2\left|\mathbf{r}_m - \mathbf{r}'_g\right|}{c}\\ n &= 1,2,\ldots,N,\ g = 1,2,\ldots,KL\end{aligned}$$

$\mathbf{x}$ is the $MN \times 1$ received vector, $\boldsymbol{\Phi}$ the measurement matrix of size $MR \times MN$ for randomly selecting frequency bins, and $\mathbf{w}$ the $MR \times 1$ noise vector, $\mathbf{r}'_g = x_g a_x + y_g a_y$ the position vector of gth pixel. Matrix $\boldsymbol{\Phi}$ could be chosen to be a matrix consisting of a single one located randomly in each row [28] so that the mutual coherence between $\boldsymbol{\Phi}$ and $\boldsymbol{\Psi}$ can be minimized. OMP reconstruction method can then be applied to recover the target scene.

3.3. Moving Target Detection Using CS

Moving target detection is considered in this section, and the second scheme of RSA, the random array mode, is used. Here RSA consists of M number of antenna elements placed in random positions. The first element of RSA acts as a transmitter (TX), and all the elements are receivers (RX), including the first one. We will look at the case of moving target detection without walls instead of the TTW case in [27].

Target scene is also divided into $K \times L$ pixels. According to [29], moving target scene can be considered sparse. The target scene at time t_i is the same as (16) and can be denoted as,

$$\mathbf{s}^i = \left[\sigma^i_{11}, \sigma^i_{21}, \ldots, \sigma^i_{K1}, \sigma^i_{12}, \sigma^i_{22}, \ldots, \sigma^i_{xy}, \ldots, \sigma^i_{KL}\right]^T \tag{19}$$

where σ^i_{xy} is the reflectivity of (x, y)th pixel at time t_i. $\sigma^i_{xy} = 0$ when no target is inside the pixel. Moving target scene at time instant t_i can be represented by the scene difference between time instants t_i and t_{i-1},

$$\mathbf{s}^i_\Delta = \mathbf{s}^i - \mathbf{s}^{i-1} = [\Delta\sigma_{11}, \Delta\sigma_{21}, \ldots, \Delta\sigma_{K1}, \Delta\sigma_{12}, \Delta\sigma_{22}, \ldots, \Delta\sigma_{KL}]^T \tag{20}$$

$$\Delta\sigma_{xy} = \sigma^i_{xy} - \sigma^{i-1}_{xy} = \begin{cases} -\sigma_q, & \text{target move out} \\ 0, & \text{no target} \\ \sigma_q, & \text{target move in} \end{cases} \tag{21}$$

Instead of being represented by summation of difference signals from all target positions, difference signal at mth RX can be represented in another form — sum of difference signals from all the KL pixel positions, including noise-only terms for non-target pixels and signal-plus-noise terms for target pixels during the observation time.

By using index g in Section 3.2, the difference signal from gth pixel position is,

$$x^i_{\Delta g}[m,n] = \Delta\sigma_g \exp(-j2\pi f_n \tau_{Tgm}) \tag{22}$$

where $\Delta\sigma_g = \Delta\sigma_{xy}$, and τ_{Tgm} is the round trip time delay from TX via gth pixel to mth RX. The total difference signal is thus in the form of (23),

$$x^i_{\Delta}[m,n] = \sum_{g=1}^{KL} \Delta\sigma_g \exp(-j2\pi f_n \tau_{Tgm}) + W_{\Delta}[m,n] \tag{23}$$

When selecting R number of frequency bins, total measurement vector becomes,

$$\mathbf{y}^i_{\Delta} = \mathbf{\Phi}\mathbf{x}^i_{\Delta} + \mathbf{w}^i_{\Delta} = \mathbf{\Phi}\mathbf{\Psi}\mathbf{s}^i_{\Delta} + \mathbf{w}^i_{\Delta} \tag{24}$$

where $\mathbf{\Phi}$ and $\mathbf{\Psi}$ are the same as (18), except the format of elements in $\mathbf{\Psi}$, $[\mathbf{\Psi}_n]_{gm} = \exp(-j2\pi f_n \tau_{Tgm})$, $\tau_{Tgm} = (|\mathbf{r}_g - \mathbf{r}'_T| + |\mathbf{r}'_m - \mathbf{r}_g|)/c$, and $\mathbf{r}_T$ is the fixed transmitter position in the RSA. $\mathbf{x}^i_{\Delta}$ is a $MN \times 1$ difference signal vector and $\mathbf{w}^i_{\Delta}$ the difference noise vector. The target scene difference $\mathbf{s}^i_{\Delta}$ could also be recovered via OMP method.

4. NUMERICAL SIMULATIONS

4.1. Static Target Detection Using RSA and CS

The system model used in the simulation consists of four point targets and a line of sampling positions along x direction. The four point targets are located inside an area of size 5 m × 5 m and range from 0 m to 5 m in x direction and 15 m to 20 m in y direction. Pixel size is set at 0.1 m × 0.1 m. All targets' reflectivities are the same ($\sigma = 1$), and other pixels have zero reflectivity ($\sigma = 0$). The exact target positions are set at (1.5, 17.9) m, (1.3, 17.5) m, (2.7, 17.5) m, and (4.1, 17.5) m, respectively. The simulation parameters are listed in Table 1, and the target scene can be found in Fig. 2(a). The aperture length of normal SAR and RSA-SAR mode is set to be the same (around 5 m). Therefore, number of sampling positions in normal SAR is much larger than that RSA requires. Results of back-projection and compressed sensing using normal SAR data and RSA data are compared. All results are shown in $[-30, 0]$ dB scale.

We choose an amount of RSA data that satisfies the measurement requirement stated in (7) and keep it to a very small value which is around 5% × 20% = 1% of full SAR data in the simulation. The number of azimuth positions in RSA is 5% of that in SAR and 20% of frequency bins are selected to form the sparse RSA data. Fig. 2 shows

Table 1. Static target simulation parameters.

Symbol	Quantity	Value
f_{st}	starting frequency	2 GHz
f_{ed}	ending frequency	3 GHz
N	number of frequency bins	201
N_s	number of azimuth positions in SAR	101
d_s	azimuth sampling spacing of SAR	50 mm
M_{RSA}	number of azimuth positions in RSA	5
r	percentage of M_{RSA}/N_s	5% of N_s
R	selected frequency bins	20% of N

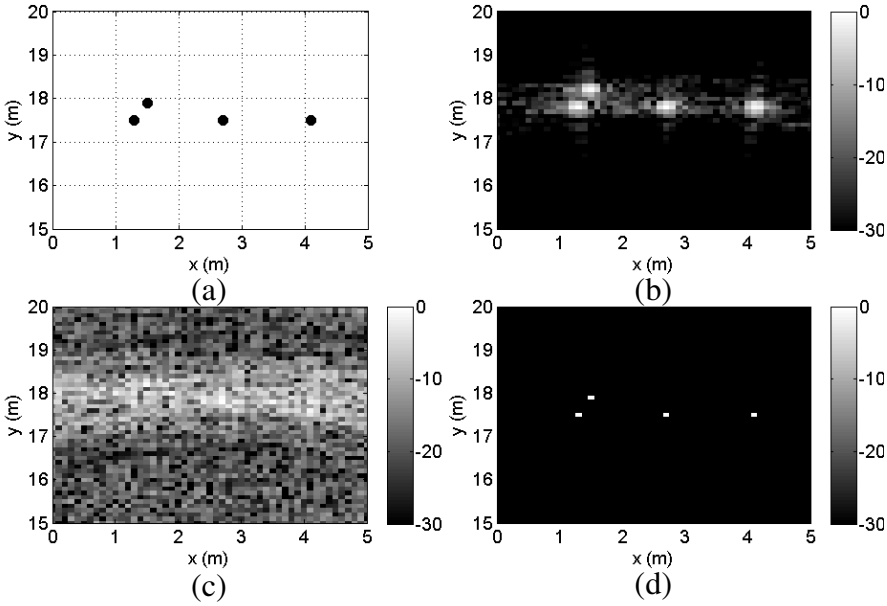

Figure 2. Static target detection results at SNR = 30 dB: (a) original target scene, (b) detection using full SAR data and back-projection, (c) detection using sparse RSA data and back-projection, (d) detection using sparse RSA data and compressed sensing.

the simulation results using full SAR data and sparse RSA data with very good signal quality. The conventional back-projection method and compressed sensing method are compared by using the same amount of sparse data.

Comparing Fig. 2(c) and Fig. 2(d), we see that using the same amount of data, compressed sensing can perform much better than

back-projection algorithm in reconstructing target scene. Although targets can be identified in Fig. 2(b), there are many sidelobes around the target positions, while detection result using RSA and compressed sensing has no sidelobes at all. This indicates that with much less

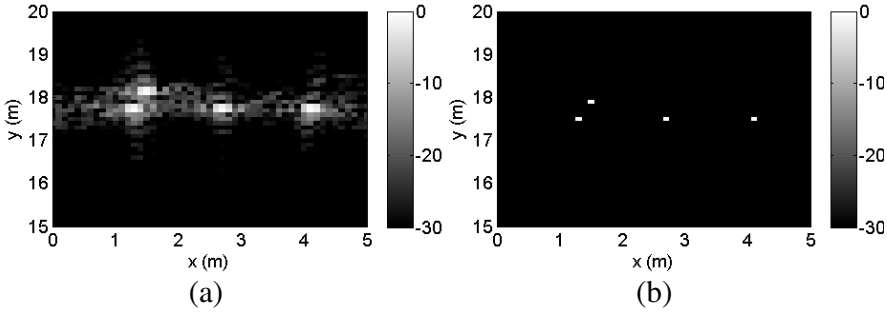

Figure 3. Detection resolutions at SNR = 0 dB: (a) back-projection with full SAR data, (b) compressed sensing with RSA data of the same size as full SAR data.

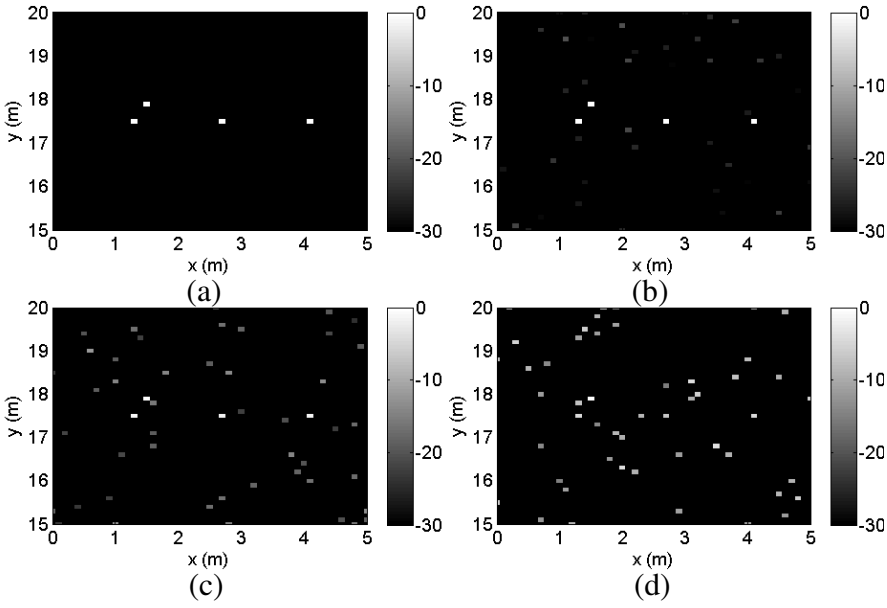

Figure 4. Static target detection results using sparse RSA data and compressed sensing at different SNR values: (a) 20 dB, (b) 10 dB, (c) 0 dB, (d) −10 dB in $[-30, 0]$ dB scale.

amount of data, RSA with compressed sensing can give much clearer detection results than normal SAR imaging method.

Beside sidelobe levels, resolution of detection is also improved. To demonstrate this, we increase the data size of RSA to the same value of SAR data, which means that RSA data has the same number of azimuth positions and frequency bins as those of SAR. The aperture of RSA is thus much larger than the aperture of SAR. A signal with relative weak quality is chosen (SNR = 0 dB). Fig. 3 gives the comparison of detection resolutions of SAR and RSA. We could observe that the resolution of target detection using RSA with compressed sensing is better improved than that using SAR with back-projection method.

However, when noise level goes up, we may see some ghost positions arise in the reconstructed image (as shown in Fig. 4). But target positions can still be seen easily when SNR is larger than -10 dB. When SNR level reaches -10 dB, targets cannot be fully detected. The image display scale in Fig. 4 is set at $[-30, 0]$ dB. To see the results more clearly, we increase the minimum display scale to -10 dB in Fig. 5.

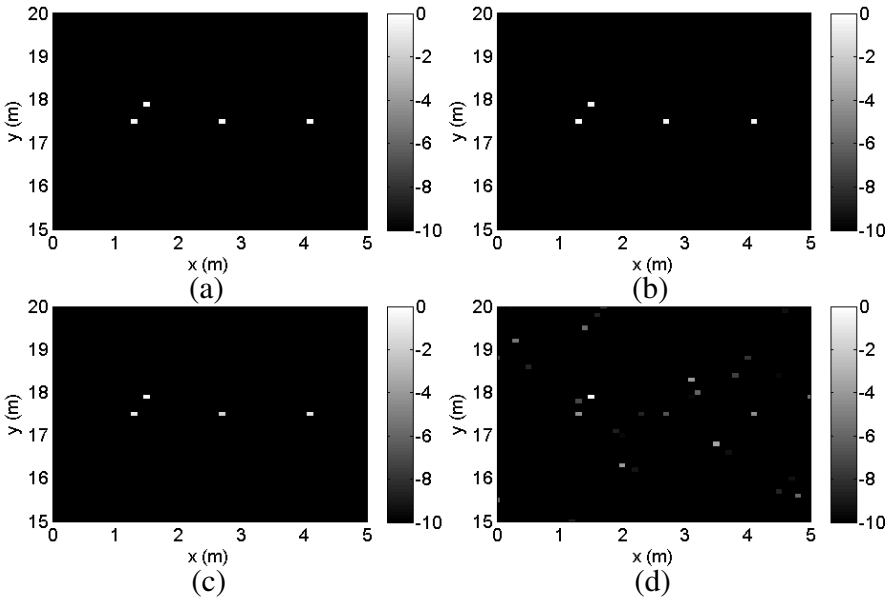

Figure 5. Static target detection results using sparse RSA data and compressed sensing at different SNR values: (a) 20 dB, (b) 10 dB, (c) 0 dB, (d) -10 dB in $[-10, 0]$ dB scale.

4.2. Moving Target Detection Using RSA and CS

RSA-array mode is used in moving target scene reconstruction. System model for moving target is shown in Fig. 6. Three targets are located in the scene with positions (1.0, 16.8) m, (1.2, 17.4) m, (2.8, 17.6) m, respectively. The first one is a static target with strong reflectivity ($\sigma = 10$) and the other two are moving targets with relatively weak reflectivity ($\sigma = 1$). Velocities of the two moving targets are assumed to be $(-2, -1)$ m/s and $(2, -1)$ m/s. After a pulse repetition interval (PRI), new positions of the two moving targets will be (1.0, 17.3) m, (3.0, 17.5) m respectively. Pixel size is still set to be 0.1 m $\times$ 0.1 m. Performance of RSA with compressed sensing is compared with that of ULA of the same aperture with conventional beamforming method. Assume that there are 5 antenna elements in the array, which is about 5% of the ULA elements with the same array aperture. 20% of frequency bins are selected. Parameters are shown in Table 2.

Table 2. Moving target simulation parameters.

Symbol	Quantity	Value
f_{st}	starting frequency	2 GHz
f_{ed}	ending frequency	3 GHz
N	number of frequency bins	201
N_a	number of antenna elements in ULA	101
d_a	array element spacing of ULA	50 mm
M_{RSA}	number of antenna elements in RSA	5
r	percentage of M_{RSA}/N_a	5% of N_a
R	selected frequency bins	20% of N
PRI	pulse repetition interval of TX	0.1 s

In this part, RSA data are again set to be 1% of ULA data, and the aperture of both RSA and ULA are kept the same for fair comparison. Moving target detection is achieved by performing change detection between two observation instants. Two positions of the targets at these two instants are reconstructed and displayed.

From the simulation results shown in Fig. 7, one can see that RSA imaging with compressed sensing can recover moving target scene perfectly with very few measurements. Conventional beamforming algorithm nearly fails when measurements are not enough. When using full ULA data of the same aperture as that of RSA, meaning much more measurements, the results are still not good compared with reconstruction result of RSA data with compressed sensing. It is also necessary to view the performance of RSA and compressed sensing

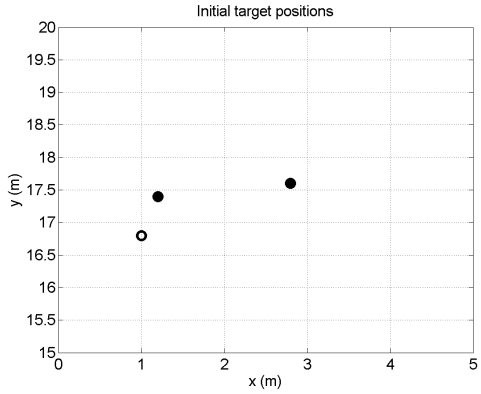

Figure 6. Original target scene (static target in black circle and moving targets in black dots).

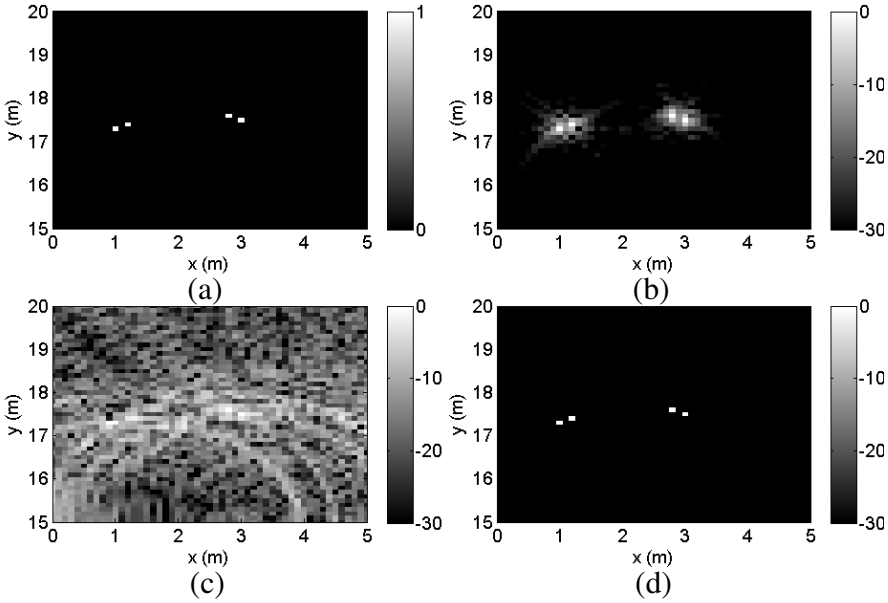

Figure 7. Moving target detection results at SNR = 30 dB: (a) moving target scene, (b) detection using full ULA data and beamforming method, (c) detection using sparse RSA data and beamforming method, (d) detection using sparse RSA data and compressed sensing.

at low SNR values. We obtain the detection results at different SNR values and compare them in Fig. 8. At SNR = −10 dB, moving targets cannot be fully detected as shown in Fig. 8(d).

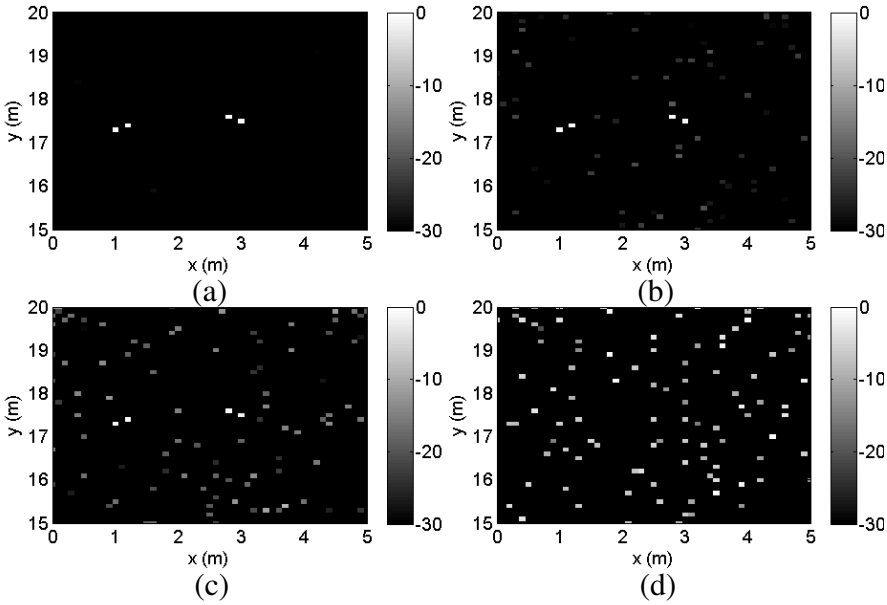

Figure 8. Moving target detection results using sparse RSA data and compressed sensing at different SNR values: (a) 20 dB, (b) 10 dB, (c) 0 dB, (d) −10 dB in $[-30, 0]$ dB scale.

5. EXPERIMENTAL RESULTS

5.1. Experimental Setup

We carried out an experimental test outside a laboratory area to verify the performance of the proposed scheme in static target detection case. Fig. 9 shows a simple SAR sensor setup consisting of two collocated broadband ridged horn antennas for transmitting and receiving, an Agilent N3382A Vector Network Analyzer (VNA) for signal generation and measurements, and a laptop with LabView software for automated measurement control. The two antennas are broadband ridged horn antennas with frequency specification from 0.8 GHz to 8.0 GHz.

The interested target scene is about 20 m long and 20 m wide. A synthesized aperture of length 13 m is used for both full SAR and RSA. The number of azimuth positions is 372, and the spacing between adjacent azimuth positions is 35 mm for SAR. The spacing between azimuth positions of RSA is random, and the number of azimuth positions in RSA is a portion of the number in SAR. A wideband signal ranging from 4 GHz to 6 GHz is synthesized by a number of frequency steps. The frequency step is 1.25 MHz, and there are 1601

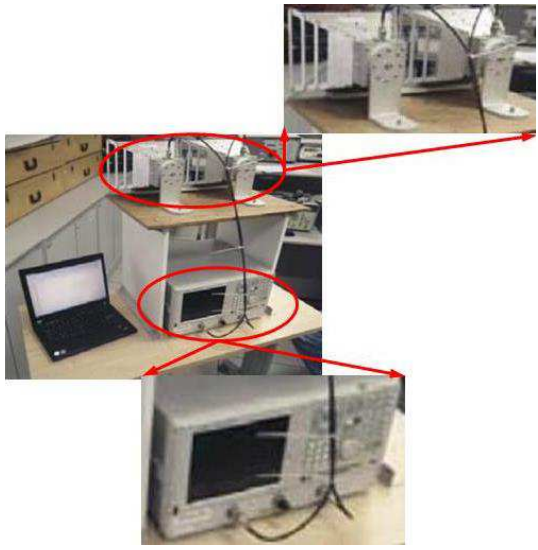

Figure 9. Equipment setup with collocated broadband transmitting and receiving antennas and an Agilent N3382A VNA as the transceiver.

Table 3. Experimental parameters.

Symbol	Quantity	Value
f_{st}	starting frequency	4 GHz
f_{ed}	ending frequency	6 GHz
N	number of frequency bins	1601
N_s	number of azimuth positions in SAR	372
d_s	azimuth sampling spacing	35 mm
M_{RSA}	number of azimuth positions in RSA	148
r	percentage of M_{RSA}/N_s	40% of N_s
R	selected frequency bins	80% of N
$\theta^{(H)}_{3\,\mathrm{dB}}$	H-plane antenna beam width	$36^\circ \pm 3^\circ$

frequency steps in total. We obtain the H-plane beam width of the antenna from its test report and list the value in Table 3 along with all other parameters. The RSA azimuth position number is 40% of that in SAR, and we choose a larger percentage (80% for instance) of selected frequency bins in the experiment for RSA to tolerant unexpected interferences or noises in the experimental case.

Figure 10 shows a photo of the ground truth that we are investigating. There are six targets in total. The four palm trees

Figure 10. Ground truth of the target area with main targets: four palm trees, one street lamp post, and one trihedral corner reflector (circled in red).

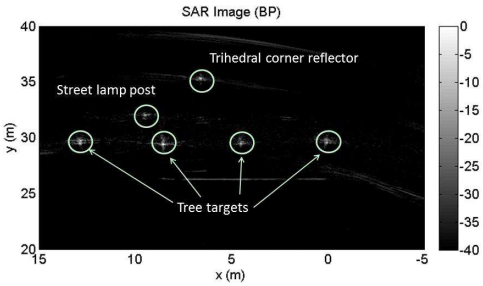

Figure 11. Imaging result using full SAR data and back-projection method with pixel size of 0.01 m × 0.01 m.

are considered as main targets. One trihedral corner reflector is placed at a position between two palm trees at the center, but a little further than them in range direction. Near the second tree from the left, there is a street lamp post made of metal and is another strong target in the scene. Fig. 11 gives the two-dimensional SAR image with a pixel size of 0.01 m × 0.01 m.

5.2. Static Target Detection Based on RSA and CS

Before presenting the experimental results, we give the respective simulation results using the same parameter set as in the experiment. As seen from Fig. 11, the six targets are located approximately at (6.6, 35) m, (9.5, 32) m, (12.8, 29.5) m, (8.5, 29.5) m, (4.5, 29.5) m and (0, 29.5) m in the sequence from further to nearer and from left to right. Fig. 12 shows the target scene and detection results using back-

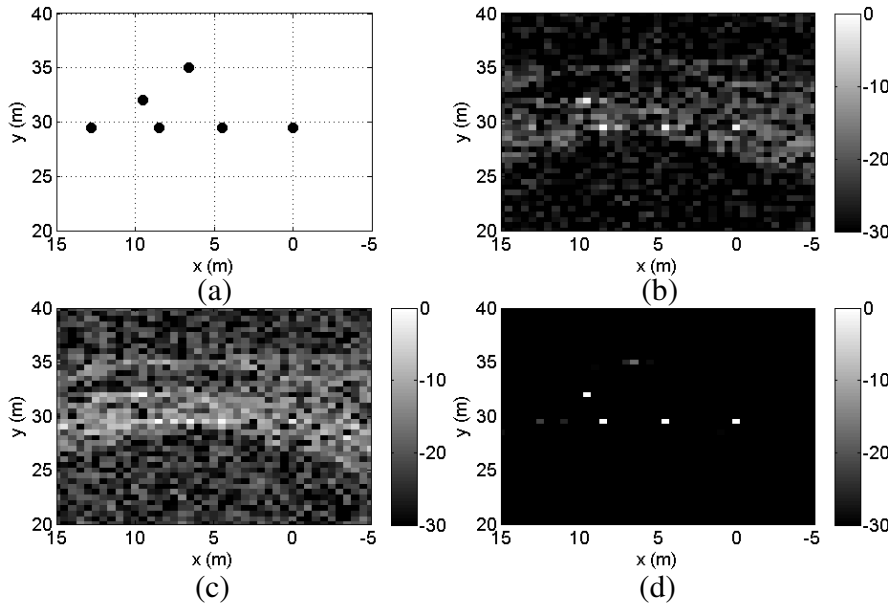

Figure 12. Static target detection results with same set of parameters as in Table 3 at SNR $= -10$ dB: (a) original target scene, (b) detection using full SAR data and back-projection, (c) detection using sparse RSA data and back-projection, (d) detection using sparse RSA data and compressed sensing.

projection method and compressed sensing. To reduce the processing time, the pixel size is set to be 0.5 m $\times$ 0.5 m in the simulation.

In the experimental results, we set the pixel size at the same value (to 0.5 m $\times$ 0.5 m) as that in Fig. 12 with the purpose of reducing processing time and giving a fair comparison. OMP algorithm is applied in compressed sensing reconstruction using RSA data. Result using full SAR data and back-projection method is shown in Fig. 13. Compared with the image in Fig. 11, the corner reflector becomes difficult to identify in this figure after pixel size is increased. Fig. 14 shows the detection result using sparse RSA data and back-projection, and Fig. 15 shows the detection result using sparse RSA data and compressed sensing.

To see the results more clearly, we decrease the image display scale of Figs. 14 and 15 to $[-10, 0]$ dB and show the resulted images in Figs. 16 and 17, respectively. Besides, we also circled necessary places in both images to emphasize the real target positions. By comparing

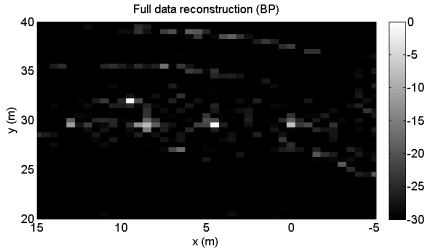

Figure 13. Detection result using back-projection with full SAR data in $[-30, 0]$ dB scale.

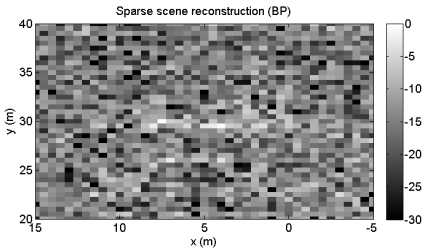

Figure 14. Detection result using back-projection with sparse RSA data in $[-30, 0]$ dB scale.

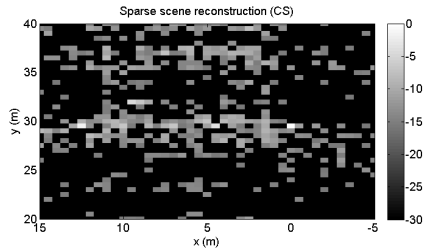

Figure 15. Detection result using compressed sensing with sparse RSA data in $[-30, 0]$ dB scale.

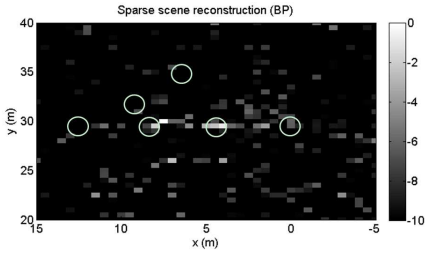

Figure 16. Detection result using back-projection with sparse RSA data in $[-10, 0]$ dB scale.

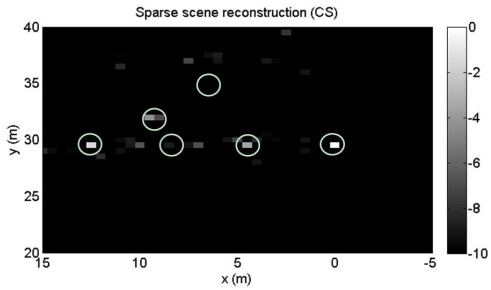

Figure 17. Detection result using compressed sensing with sparse RSA data in $[-10, 0]$ dB scale.

these two figures, we can see that compressed sensing with sparse RSA data produces better result in Fig. 17 than back-projection with the same sparse data in Fig. 16. In Fig 17, the lamp is recognizable. Four palm trees can still be identified in the image except the one nearest

to the lamp. This is possibly due to the strong reflections of the lamp which submerges the reflection of the second palm tree. The corner reflector is totally missed due to weak reflection. Targets in Fig. 16 are not recognizable at all.

When comparing the result in Fig. 17 with that in Fig. 13, we find that detection result of compressed sensing with sparse RSA data is not as good as that using back-projection method with full SAR data. In this case, from the viewpoint of perfect target detection, full SAR method gives much better result than RSA and compressed sensing. It is concluded that in practical experiments, target detection using compressed sensing and RSA may not be ideal, but it decreases data storage and processing time with acceptable performance. Targets may not be fully and correctly detected when the environment consists of many unknown sources, possibly including the undesired reflections and possible multiple scattering from the static background. When data storage and processing time are not the concern, back-projection method with more SAR data may have better detection result than compressed sensing method with less RSA data.

6. CONCLUSIONS

In this paper, a target detection method based on random sparse array (RSA) and compressed sensing imaging is presented and evaluated. Simulated and experimental examples are presented to validate the method. The results show that the two proposed RSA schemes combined with compressed sensing can achieve higher resolution and lower sidelobe levels than traditional imaging methods in both static and moving target detections. However, the performance of RSA with compressed sensing is degraded for real situations since environment is complex with many unknown sources, and further studies are needed to improve the algorithms for real applications.

REFERENCES

1. Candes, E., J. Romberg, and T. Tao, "Robust uncertainty principles: Exact signal reconstruction from highly incomplete frequency information," *IEEE Trans. Inf. Theory*, Vol. 52, 489–509, Feb. 2006.
2. Candes, E., J. Romberg, and T. Tao, "Stable signal recovery from incomplete and inaccurate measurements," *Comm. Pure Appl. Math.*, Vol. 59, 1207–1223, Mar. 2006.
3. Donoho, D., "Compressed sensing," *IEEE Trans. Inf. Theory*, Vol. 52, 1289–1306, Apr. 2006.

4. Baraniuk, R. and P. Steeghs, "Compressive radar imaging," *Proc. 2007 IEEE Radar Conference*, 128–133, 2007.
5. Patel, V. M., G. R. Easley, D. M. Healy, and R. Chellappa, Jr., "Compressed synthetic aperture radar," *IEEE J. Sel. Topics Signal Process.*, Vol. 4, No. 2, 244–254, Apr. 2010.
6. Wei, S. J., X. L. Zhang, J. Shi, and G. Xiang, "Sparse reconstruction for SAR imaging based on compressed sensing," *Progress In Electromagnetics Research*, Vol. 109, 63–81, 2010.
7. Alonso, M. T., P. López-Dekker, and J. J. Mallorquí, "A novel strategy for radar imaging based on compressive sensing," *IEEE Trans. Geosci. Remote Sens.*, Vol. 48, No. 12, 4285–4295, Dec. 2010.
8. Wei, S. J., X. L. Zhang, and J. Shi, "Linear array SAR imaging via compressed sensing," *Progress In Electromagnetics Research*, Vol. 117, 299–319, 2011.
9. Li, J., S. Zhang, and J. Chang, "Applications of compressed sensing for multiple transmitters multiple azimuth beams SAR imaging," *Progress In Electromagnetics Research*, Vol. 127, 259–275, 2012.
10. Yang, J. G., J. Thompson, X. T. Huang, T. Jin, and Z. M. Zhou, "Random-frequency SAR imaging based on compressed sensing," *IEEE Trans. Geosci. Remote Sens.*, 1–12, 2012.
11. Kurtz, J. L. and R. J. Tan, "Sparse array of RF sensors for sensing through the wall," *Proc. SPIE*, Vol. 6547, 5470B1–11, 2007.
12. Ao, Z. J., L. J. Kong, Y. Jia, and J. Y. Yang, "Multi-channel target cooperative detection in through-the-wall-radar imaging based on random sparse array," *IEEE CIE International Conference on Radar*, Vol. 1, 176–178, 2011.
13. Carin, L., "On the relationship between compressive sensing and random sensor arrays," *IEEE Antennas Propagat. Mag.*, Vol. 51, 72–81, 2009.
14. Carin, L., L. Dehong, and G. Bin, "Coherence, compressive sensing, and random sensor arrays," *IEEE Antennas Propagat. Mag.*, Vol. 53, 28–39, 2011.
15. Soumekh, M., *Synthetic Aperture Radar Signal Processing with MATLAB Algorithms*, Wiley, 1999.
16. Marcelo, A., P. Pau, and S. Rolf, "Applications of time-domain back-projection SAR processing in the airborne case," *Proc. 7th European Conference on Synthetic Aperture Radar*, 1–4, Jun. 2008.
17. Donoho, D., M. Elad, and V. N. Temlyakov, "Stable recovery

of sparse overcomplete representations in the presence of noise," *IEEE Trans. Inf. Theory*, Vol. 52, No. 1, 6–18, Jan. 2006.

18. Candes, E. and J. Romberg, "Sparsity and incoherence in compressed sensing," *Inverse Problems*, Vol. 23, 2006.
19. Goldstein, T. and S. Osher, "The split Bregman method for L1-regularized problems," *SIAM Journal on Imaging Sciences*, Vol. 2, 285–322, 2009.
20. Romberg, J., "L1-magic," Aug. 2008, available: http://www.acm.caltech.edu/l1magic/.
21. Mallat, S., *A Wavelet Tour of Signal Processing*, Academic Press, 1999.
22. Needell, D. and R. Vershynin, "Uniform uncertainty principle and signal recovery by regularization orthogonal matching pursuit," *Journal Foundations of Computational Mathematics*, Vol. 9, Apr. 2009.
23. Needell, D. and R. Vershynin, "Greedy signal recovery and uncertainty principles," *Proc. SPIE*, 68140J, Bellingham, WA, 2008.
24. Donoho, D. L., I. Drori, Y. Tsaig, and J. L. Starck, "Sparse solution of underdetermined systems of linear equations by stagewise orthogonal matching pursuit," *IEEE Trans. Inf. Theory*, Vol. 58, 1094–1121, Feb. 2012.
25. Dissanayake, G., S. Sukkarieh, E. Nebot, and H. Durrant-Whyte, "The aiding of a low-cost strapdown inertial measurement unit using vehicle model constraints for land vehicle applications," *IEEE Trans. Robot. Automat.*, Vol. 17, 731–747, 2001.
26. Cao, F. X., D. K. Yang, A. G. Xu, J. Ma, W. D. Xiao, C. L. Law, K. V. Ling, and H. C. Chua, "Low cost SINS/GPS integration for land vehicle navigation," *Proc. ITSC 2002*, 910–913, 2002.
27. Huang, L. and Y. L. Lu, "Radar imaging with compressed sensing for detecting moving targets behind walls," *IET International Conference on Radar Systems*, 2012.
28. Yoon, Y.-S. and M. G. Amin, "Compressed sensing technique for high-resolution radar imaging," *Proc. SPIE*, Vol. 6968, 696 81A.1–696 81A.10, May 2008.
29. Amin, M., F. Ahmad, and W. J. Zhang, "A compressive sensing approach to moving target indication for urban sensing," *Proc. 2011 IEEE Radar Conference*, 509–512, 2011.